Semaphorin 3E–Plexin-D1 signaling controls pathway-specific synapse formation in the striatum

Jun B Ding[1–3], Won-Jong Oh[1,3], Bernardo L Sabatini[1,2] & Chenghua Gu[1]

The proper formation of synaptic connectivity in the mammalian brain is critical for complex behavior. In the striatum, balanced excitatory synaptic transmission from multiple sources onto two classes of principal neurons is required for coordinated and voluntary motor control. Here we show that the interaction between the secreted semaphorin 3E (Sema3E) and its receptor Plexin-D1 is a critical determinant of synaptic specificity in cortico-thalamo-striatal circuits in mice. We find that *Sema3e* (encoding Sema3E) is highly expressed in thalamostriatal projection neurons, whereas in the striatum *Plxnd1* (encoding Plexin-D1) is selectively expressed in direct-pathway medium spiny neurons (MSNs). Despite physical intermingling of the MSNs, genetic ablation of *Plxnd1* or *Sema3e* results in functional and anatomical rearrangement of thalamostriatal synapses specifically in direct-pathway MSNs without effects on corticostriatal synapses. Thus, our results demonstrate that Sema3E and Plexin-D1 specify the degree of glutamatergic connectivity between a specific source and target in the complex circuitry of the basal ganglia.

One of the noteworthy features of the central nervous system is the precision of synaptic connections, which is essential for the proper formation of functional circuits and the generation of complex behavior and cognitive function. During development, after axons have navigated long distances to reach their targets, they choose appropriate synaptic partners and, in many cases, also select a domain of the postsynaptic cell on which to form synapses[1,2]. The challenges of achieving the proper synapse specificity of wiring in the mammalian brain are evident in the striatum. As the input nucleus of the basal ganglia, the striatum receives convergent excitatory inputs carrying motor, sensory and cognitive information from the cortex and thalamus. Specific excitatory synaptic connections need to be formed between axons arising from these two areas and two functionally distinct but anatomically intermingled populations of targets, direct and indirect pathway striatal MSNs[3]. The proper balance of excitatory synaptic transmission onto direct and indirect pathway MSNs is required for coordinated and voluntary motor function, and imbalances of synaptic strength are thought to contribute to neuropsychiatric diseases such as Parkinson's disease and attention deficit hyperactivity disorder[4].

Direct and indirect pathway MSNs are functionally and molecularly distinct, despite being physically intermixed and having similar electrophysiological and morphological properties[5,6]. Direct pathway MSNs express type 1 dopamine receptors (*Drd1a*) and their activity promotes motor action, whereas indirect pathway MSNs express type 2 dopamine receptors (*Drd2*) and their activity suppresses action initiation[7]. Individual direct and indirect pathway MSNs receive input from both cortex and thalamus[8–11]; likewise, individual cortical and thalamic axons innervate both classes of MSN[10,11]. However, cortical and thalamic projections differ in several aspects. Cortical boutons express the vGluT1 vesicular glutamate transporter, have lower probability of release and nearly always form synapses onto the heads

of dendritic spines. In contrast, thalamic axons express the vGluT2 vesicular glutamate transporter, have higher probability of release and form fewer synapses, which are nearly equally distributed between the dendritic shaft and dendritic spine heads[9,11,12].

Our understanding of synapse specification—that is, how a specific synaptic target is selected from among many—mainly arises from studies of laminar specificity. In some parts of the mammalian CNS such as the retina and hippocampus, functionally similar neuronal subtypes are anatomically segregated and arranged into a stereotypic laminar organization. A prevailing model emerging from studies of *Caenorhabditis elegans* and of laminar specificity in the retina is that synapse specificity is established by a direct interaction between presynaptic and postsynaptic protein partners that comprise a complementary set of recognition molecules[1,13–18]. These signaling pairs can mediate positive adhesive interactions that direct axons to particular laminae. Alternatively, postsynaptic target laminae establish a concentration gradient of secreted or transmembrane proteins to repel innervation by inappropriate inputs. However, in many regions of the mammalian brain including the striatum, heterogeneous populations of neurons are intermingled, rendering secretion of a repellent signal by target neurons insufficient to direct synapse selection.

In this study, we find that the *in vivo* interaction between a traditional axon repulsive cue, Sema3E, and its receptor, Plexin-D1, determines synaptic specificity in cortico-thalamo-striatal circuits. We show that Sema3E is secreted by thalamostriatal axons and Plexin-D1 is selectively expressed by one subtype of postsynaptic neuron, the direct pathway MSN. Genetic ablation of *Plxnd1* or *Sema3e* affects glutamatergic synapses formed onto direct pathway MSNs without affecting synapses onto indirect pathway MSNs. Furthermore, electrophysiological and optogenetic analyses reveal that thalamostriatal innervation of direct pathway MSNs is specifically strengthened in

[1]Department of Neurobiology, Harvard Medical School, Boston, Massachusetts, USA. [2]Howard Hughes Medical Institute, Harvard Medical School, Boston, Massachusetts, USA. [3]These authors contributed equally to this work. Correspondence should be addressed to B.L.S. (bernardo_sabatini@hms.harvard.edu) or C.G. (chenghua_gu@hms.harvard.edu).

Plxnd1 mutant mice. These changes are accompanied by increased density of immunohistochemical markers of thalamostriatal synapses onto direct pathway MSNs, indicating that Sema3E–Plexin-D1 signaling normally restricts the number of these synapses. Thus, Sema3E and Plexin-D1 serve as a molecular recognition system to control specific synaptic connections in the complex circuitry of the basal ganglia.

RESULTS

Complementary expression of *Sema3e* and *Plxnd1*

We found complementary patterns of expression of *Sema3e* and *Plxnd1* in the cortex-thalamus-striatum circuit (**Fig. 1**). *In situ* hybridization (ISH) revealed that *Plxnd1* was highly expressed in the striatum at postnatal day (P) 3 (**Fig. 1a,b**). Conversely, *Sema3e* was expressed in the thalamus and sparsely in deep cortical layers, the two principal sources of glutamatergic inputs to the striatum. *In vivo* retrograde labeling of thalamostriatal projection neurons with DiI and subsequent *Sema3e* ISH revealed that *Sema3e* was expressed in many of these neurons, particularly in the parafascicular and centromedian intralaminar nuclei (**Fig. 1c,d**), the main thalamic nuclei that project to the striatum[9]. Neuropilin-1, a co-receptor for Sema3E that modulates Sema3E–Plexin-D1 signaling in other systems[19], was absent in the striatum (**Supplementary Fig. 1**), suggesting that Plexin-D1 acts independently as a receptor for Sema3E in this brain region.

Striatal *Plxnd1* expression was maintained during early postnatal life (P0–P8; **Fig. 1e,f**) and diminished to undetectable levels by P14–P25 (**Supplementary Fig. 2**). Thus, *Plxnd1* is expressed in the striatum during the developmental stage when initial synaptogenesis occurs[20–22]. The postnatal and complementary expression patterns of *Plxnd1* and *Sema3e* in the striatum and thalamostriatal projecting neurons, respectively, suggest that they may influence the formation and refinement of glutamatergic synapses.

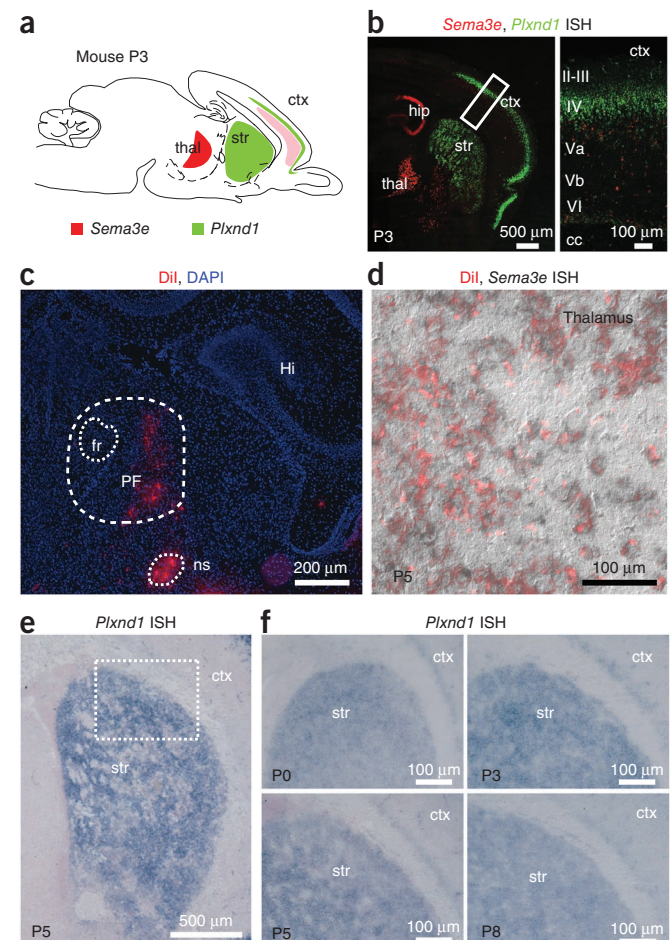### Plexin-D1 is selectively expressed in direct pathway MSNs

To determine whether *Plxnd1* is expressed selectively in one class of MSNs, we used double fluorescence ISH to examine the expression of *Plxnd1* in the striatum of transgenic mice that exploit the cell-type specific expression of dopamine receptor subtypes to express GFP by means of a bacterial artificial chromosome (BAC) selectively in either direct pathway (*Drd1a-GFP*) or indirect pathway (*Drd2-GFP*) MSNs (**Fig. 2** and **Supplementary Fig. 3**)[23]. In P3 *Drd1a-GFP* mice, the expression of *Plxnd1* in the striatum overlapped with that of *GFP*, such that ~85% of all direct pathway MSNs expressed *Plxnd1* (**Fig. 2a,c**). In contrast, *Plxnd1* expression did not overlap with that of *GFP* in *Drd2-GFP* mice (**Fig. 2b,c**), indicating an absence of expression in indirect pathway MSNs. The cell-by-cell correlation coefficients of *GFP* and *Plxnd1* expression levels were 0.8 in *Drd1a-GFP* and 0.1 in *Drd2-GFP* mice (n = 7 sections; P < 0.05, Mann-Whitney; **Fig. 2d**).

To confirm that most *Plxnd1* expression is confined to direct pathway MSNs, we quantified *Plxnd1* in the striatum of mice in which *Plxnd1* was selectively deleted in direct or indirect pathway MSNs by crossing mice carrying a *loxP*-flanked ('floxed') *Plxnd1* gene (*Plxnd1^{f/f}* mice) with *Drd1a-cre* or *Drd2-cre* mice, respectively. *Drd2-GFP;Drd1a-cre;Plxnd1^{f/f}* (referred to as direct pathway mutant) and *Drd2-GFP;Drd2-cre;Plxnd1^{f/f}* (indirect pathway mutant) mice were viable and fertile, permitting studies of synapse formation at postnatal stages. ISH revealed that striatal *Plxnd1* expression was significantly reduced in direct pathway mutant mice compared to wild-type littermate controls (8.7% ± 2.9% of control, n = 12 and n = 10 sections from control and *Drd1a-cre;Plxnd1^{f/f}* mice, respectively; P < 0.05, Mann-Whitney; **Fig. 2e,f**). In contrast, there was no difference in *Plxnd1* expression in indirect pathway mutant mice (86.1% ± 7.6% of control, n = 6 sections each from control and *Drd2-cre;Plxnd1^{f/f}* mice; P > 0.05, Mann-Whitney; **Fig. 2g,h**). These data demonstrate that, in the striatum, *Plxnd1* is expressed selectively in direct pathway MSNs and is thus a potential molecular cue to differentially control glutamatergic synapse formation onto these two cell classes.

Deletion of *Plxnd1* or *Sema3e* perturbs synapse function

To test whether *Sema3e* and *Plxnd1* are required for synapse formation *in vivo*, we examined glutamatergic synapses onto direct and indirect MSNs in the pathway-specific *Plxnd1* conditional knockout mice (direct pathway mutant *Drd2-GFP;Drd1a-cre;Plxnd1^{f/f}* and indirect pathway mutant *Drd2-GFP;Drd2-cre;Plxnd1^{f/f}*). The use of *Drd2-GFP* mice enables identification of direct and indirect pathway MSNs in the striatum based on the absence and presence, respectively,
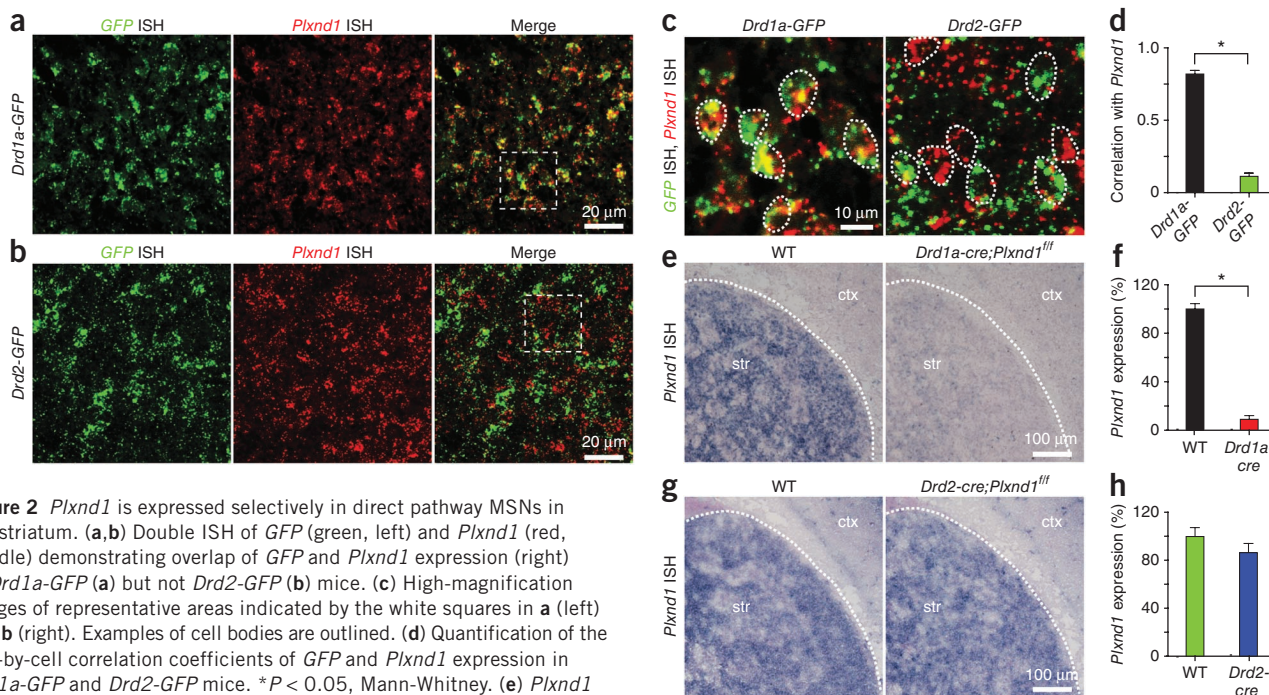

Figure 1 Complementary expression pattern of *Sema3e* and *Plxnd1* in the cortex-thalamus-basal ganglia circuit. (**a**) Schematic of a sagittal section of the mouse brain depicting the areas of expression of *Sema3e* and *Plxnd1*. Ctx, cortex; thal, thalamus; str, striatum. (**b**) Two-color double ISH on P3 pups showing the expression pattern of *Sema3e* and *Plxnd1*. *Sema3e* is highly expressed in thalamic neurons (red), whereas *Plxnd1* is highly expressed in the striatum and the cortex (green, left). Note layer-specific expression of *Sema3e* (low and sparse expression in deep layers) and *Plxnd1* (dense layer 4) in cortex (right). Hip, hippocampus; cc, corpus callosum. (**c**) Labeling of thalamostriatal projection neurons in a P5 mouse brain after DiI (red) injection into the striatum at P3. The parafascicular nucleus (PF), nigrostriatal bundle (ns), fasciculus retroflexus (fr) and hippocampus (Hi) are labeled. (**d**) DiI-labeled thalamostriatal projection neurons (red) express *Sema3e*, as shown by ISH (black). (**e,f**) *Plxnd1* is highly expressed throughout the postnatal striatum until at least P8.

Figure 2 *Plxnd1* is expressed selectively in direct pathway MSNs in the striatum. (**a**,**b**) Double ISH of *GFP* (green, left) and *Plxnd1* (red, middle) demonstrating overlap of *GFP* and *Plxnd1* expression (right) in *Drd1a-GFP* (**a**) but not *Drd2-GFP* (**b**) mice. (**c**) High-magnification images of representative areas indicated by the white squares in **a** (left) and **b** (right). Examples of cell bodies are outlined. (**d**) Quantification of the cell-by-cell correlation coefficients of *GFP* and *Plxnd1* expression in *Drd1a-GFP* and *Drd2-GFP* mice. *$P < 0.05$, Mann-Whitney. (**e**) *Plxnd1* mRNA expression in a *Drd1a-cre;Plxnd1$^{f/f}$* mouse compared to its wild-type (WT) littermate control. Ctx, cortex; str, striatum. (**f**) Quantification of *Plxnd1* expression shows a significant drop of *Plxnd1* expression in *Drd1a-cre;Plxnd1$^{f/f}$* mice. *$P < 0.05$, Mann-Whitney. (**g**) Similar analysis using *Drd2*-Cre mice demonstrates *Plxnd1* expression is unchanged in *Drd2-cre; Plxnd1$^{f/f}$* mice compared to WT control. (**h**) Quantification of *Plxnd1* expression in *Drd2-cre;Plxnd1$^{f/f}$* and WT control mice. Error bars denote s.e.m.

of GFP expression. To determine whether deletion of *Plxnd1* alters the numbers of glutamatergic synapses formed onto MSNs, we examined two proxies of synapse number. First, to assess the number of active synapses, we measured AMPA receptor–mediated spontaneous miniature excitatory postsynaptic currents (mEPSCs) using whole-cell voltage-clamp recordings. Loss of *Plxnd1* in direct pathway MSNs led to a large and significant ($P < 0.05$, Mann-Whitney) increase in mEPSC frequency in direct pathway MSNs (direct pathway mutant, 2.20 ± 0.25 Hz; $n = 12$ cells) compared to either Cre-negative (*Plxnd1$^{f/f}$* (*f/f* ctrl), 1.39 ± 0.21 Hz; $n = 6$ cells) or Cre-positive control neurons (*Drd1a-cre;Plxnd1$^{f/+}$* (het ctrl), 1.07 ± 0.14 Hz; $n = 12$ cells) without significant changes in mEPSC amplitude (10.9 ± 0.5 pA; *f/f* ctrl, 10.3 ± 1.1 pA; het ctrl, 10.1 ± 0.3 pA; direct pathway mutant. 10.9 ± 0.5 pA; $P > 0.05$, Mann-Whitney) (**Fig. 3a–c**). Similar analysis demonstrated that loss of *Plxnd1* in indirect pathway MSNs did not cause significant changes in mEPSC frequency (*f/f* ctrl, 2.14 ± 0.37 Hz, $n = 5$ cells; het ctrl, 1.99 ± 0.17 Hz, $n = 10$ cells; indirect pathway mutant, 2.11 ± 0.16 Hz, $n = 8$ cells; $P > 0.05$, Mann-Whitney) or amplitude (*f/f* ctrl, 12.0 ± 1.1 pA; het ctrl, 10.9 ± 0.6 pA; indirect pathway mutant, 11.0 ± 0.5 pA; $P > 0.05$, Mann-Whitney) (**Fig. 3d–f**). These results suggest that loss of *Plxnd1* increases presynaptic vesicular release probability or the number of active glutamatergic synapses formed onto direct pathway MSNs without effect on indirect pathway MSNs, indicating that Plexin-D1 negatively regulates synapses in direct pathway MSNs.

Second, we imaged MSNs in acute brain slices using two-photon laser-scanning microscopy (2PLSM) to measure the density of dendritic spines. In MSNs, the large majority of cortical glutamatergic inputs are formed onto dendritic spines and the majority of spines are associated with corticostriatal synapses, such that changes in the number of spines are thought to parallel changes in the number of corticostriatal synapses. We filled *Plxnd1* null and control MSNs with the red fluorophore Alexa Fluor-594 through a whole-cell

recording pipette and imaged dendritic branches (50–80 μm from soma) (**Fig. 4a**). To our surprise, in contrast to the increase in frequency of mEPSCs, loss of *Plxnd1* in direct pathway MSNs led to a small (~17%) but significant ($P < 0.05$, Mann-Whitney) decrease in spine density in direct pathway MSNs (0.87 ± 0.03 spines μm^{-1}; $n = 38$ dendrites in 9 cells) compared to control direct pathway neurons (*f/f* ctrl, 1.10 ± 0.03 spines μm^{-1}, $n = 16$ dendrites in 6 cells; het ctrl, 1.05 ± 0.03 spines μm^{-1}, $n = 35$ dendrites in 8 cells; **Fig. 4b,c**). Similar analysis of MSNs in indirect pathway mutants revealed no change ($P > 0.05$, Mann-Whitney) in spine density (*f/f* ctrl, 1.06 ± 0.03 spines μm^{-1}, $n = 16$ dendrites in 5 cells; het ctrl, 1.11 ± 0.04 spines μm^{-1}, $n = 19$ dendrites in 6 cells; indirect pathway mutant, 1.02 ± 0.03 spines μm^{-1}, $n = 32$ dendrites in 8 cells; **Fig. 4b,c**). No significant changes in spine length, width or head area were observed in either mutant (**Supplementary Fig. 4**).

To test whether loss of Plexin-D1 affects dendrite morphology, we traced Alexa Fluor-594–filled striatal MSNs and measured dendritic length and branching (**Supplementary Fig. 5**). In the absence of *Plxnd1*, Scholl analysis revealed a slight increase in complexity of dendrites in direct pathway MSNs ($P < 0.05$ for dendritic segments 70–95 μm from soma; $n = 10$ in control and 11 in mutant mice; Mann-Whitney) but not in the indirect pathway MSNs (**Supplementary Fig. 5**). The resulting small increase in total dendrite length counteracted the decreased dendritic spine density such that estimates of the total spine number (density × length) were similar in control and *Plxnd1*-lacking direct pathway MSNs ($1,591.8 \pm 74.3$ and $1,496.4 \pm 127.4$ spines, respectively). These data indicate that the large increase in mEPSC frequency in direct pathway MSNs caused by loss of Plexin-D1 is accompanied by only minor structural changes and is thus unlikely to result from a greater number of glutamatergic synapses formed on dendritic spines.

To determine whether Sema3E, a known Plexin-D1 ligand[24], is required for synapse formation in direct pathway MSNs, we analyzed
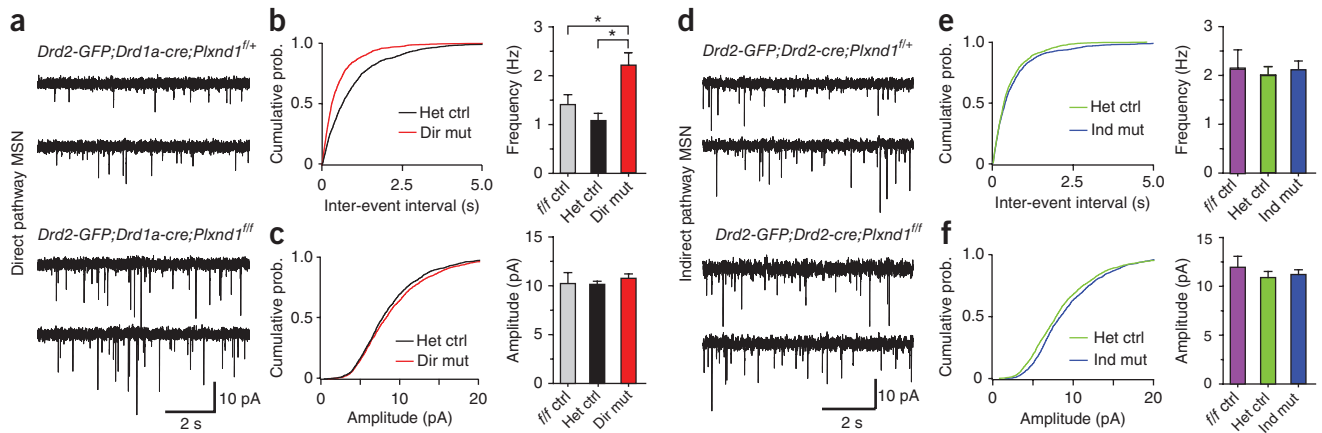
Figure 3 Deletion of *Plxnd1* markedly increases mEPSC frequency in direct pathway MSNs. (**a**) Traces showing mEPSCs recorded from direct pathway MSNs from *Drd2-GFP;Drd1a-cre;Plxnd1* conditional littermate control (top) and knockout mice (bottom). (**b**) Cumulative probability (prob.) plots of mEPSC inter-event intervals (left) and summary of mean mEPSC frequency (right) in direct pathway MSNs. Dir mut, direct pathway mutant. *$P < 0.05$, Mann-Whitney. (**c**) Cumulative probability plots of mEPSC amplitudes (left) and summary of mean mEPSC amplitude (right) in direct pathway MSNs. (**d**) Traces showing mEPSCs recorded from indirect pathway MSNs from *Drd2-GFP;Drd2-cre;Plxnd1* littermate control (top) and conditional knockout (bottom) mice. (**e**) Cumulative probability plots of mEPSC inter-event intervals (left) and summary of mean mEPSC frequency (right) in indirect pathway MSNs. Ind mut, indirect pathway mutant. (**f**) Cumulative probability plots of mEPSC amplitudes (left) and summary of mean mEPSC amplitude (right) in indirect pathway MSNs. Error bars denote s.e.m.

mEPSCs and spine density in *Drd2-GFP;Sema3e$^{-/-}$* mice. Loss of *Sema3e* caused similar synapse number and spine density phenotypes as loss of *Plxnd1* in MSNs *in vivo*: increased mEPSC frequency (control, 0.88 ± 0.13 Hz, $n = 5$; *Sema3e$^{-/-}$*, 1.61 ± 0.15 Hz, $n = 6$; $P < 0.05$, Mann-Whitney) without change in amplitude (control, 11.1 ± 0.5 pA, $n = 5$; *Sema3e$^{-/-}$*, 10.1 ± 0.6 pA; $P > 0.05$, Mann-Whitney; **Fig. 5a,b**). These synaptic phenotypes were only seen in direct pathway MSNs; in indirect pathway MSNs, the mEPSC frequency (control, 2.01 ± 0.25 Hz, $n = 6$; *Sema3e$^{-/-}$*, 2.13 ± 0.53 Hz, $n = 7$; $P > 0.05$, Mann-Whitney) and amplitude (control, 10.8 ± 0.7 pA; *Sema3e$^{-/-}$*, 10.8 ± 1.3 pA; $P > 0.05$, Mann-Whitney; **Fig. 5c,d**). Morphological analysis revealed an ~15% decrease in spine density in direct but not indirect pathway MSNs (direct pathway: control *Drd2-GFP;Sema3e$^{+/+}$*, 1.08 ± 0.04 spines µm^{-1}, $n = 24$ dendrites in 6 cells; *Drd2-GFP;Sema3e$^{-/-}$*, 0.92 ± 0.03 spines µm^{-1}, $n = 27$ dendrites in 7 cells; $P < 0.05$,

Mann-Whitney; indirect pathway: control *Drd2-GFP;Sema3e$^{+/+}$*, 1.06 ± 0.03 spines µm^{-1}, $n = 34$ dendrites in 7 cells; *Drd2-GFP;Sema3e$^{-/-}$*, 1.08 ± 0.05 spines µm^{-1}, $n = 27$ dendrites in 8 cells; $P < 0.05$, Mann-Whitney; **Fig. 5e,f**) without changes in spine morphology (**Supplementary Fig. 6**). Thus, loss of Sema3E selectively alters glutamatergic synapses in direct pathway MSNs, phenocopying the effects of Plexin-D1 loss. These results support the conclusion that Sema3E is the ligand for Plexin-D1 in the striatum and that the interaction between Sema3E and Plexin-D1 controls synapse formation in the direct pathway MSNs.

Postnatal *Plxnd1* expression regulates synapse formation
Although it is possible that the synaptic defects observed in the *Plxnd1* conditional knockout mice are due to loss of *Plxnd1* function in early development, rather than a direct function of Plexin-D1
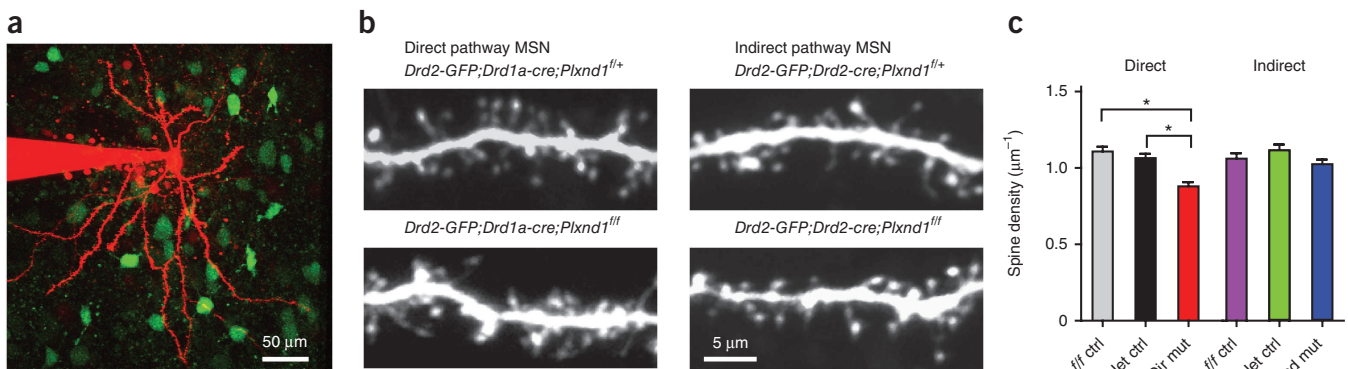
Figure 4 Deletion of *Plxnd1* slightly decreases spine density in direct pathway MSNs. (**a**) 2PLSM image of a brain slice from a *Drd2-GFP;Drd1a-cre;Plxnd1$^{f/+}$* mouse showing GFP-expressing indirect pathway MSNs (green) and one MSN that was filled with Alexa Fluor-594 (red) through the whole-cell recording pipette. (**b**) High-magnification images of spiny dendritic segments of direct (left) and indirect (right) pathway MSNs in mice that have selectively lost one (top) or both (bottom) copies of *Plxnd1* in MSNs of each pathway. Direct pathway MSNs in *Drd2-GFP;Drd1a-cre;Plxnd1$^{f/f}$* mice show decreased spine density compared to their littermate controls. In contrast, indirect pathway MSNs in *Drd2*-specific *Plxnd1* knockout mice (*Drd2-GFP;Drd2-cre;Plxnd1$^{f/f}$*) show no difference in spine density compared to their littermate controls (*Drd2-GFP;Drd2-cre;Plxnd1$^{f/+}$*). (**c**) Summary of spine densities in direct and indirect pathway MSNs of the indicated genotypes. Dir mut, direct pathway mutant; ind mut, indirect pathway mutant. There was a small but significant loss of spines in direct pathway MSNs in *Drd1a-cre Plxnd1* conditional knockout mice compared to Cre$^-$ (*f/f* ctrl) and Cre$^+$ (het ctrl) control mice. *$P < 0.05$, Mann-Whitney. Error bars denote s.e.m.

Figure 5 Deletion of *Sema3e* increases mEPSC frequency and decreases spine density in direct pathway MSNs. (**a**) Traces showing mEPSCs recorded from direct pathway MSNs from *Drd2-GFP;Sema3e+/+* (left) and *Drd2-GFP;Sema3e−/−* (right) mice. (**b**) Summary of mean mEPSC frequency (left) and amplitude (right) in direct pathway MSNs. (*P < 0.05, Mann-Whitney). (**c**) Traces showing mEPSCs recorded from indirect pathway MSNs from *Drd2-GFP;Sema3e+/+* (top) and *Drd2-GFP;Sema3e−/−* (right) mice. (**d**) Summary of mean mEPSC frequency (left) and amplitude (right) indirect pathway MSNs. (**e**) Images of spiny dendrites of direct (top) and indirect (right) pathway MSNs in wild-type (left) and *Sema3e−/−* (right) mice. (**f**) Summary of spine densities in direct and indirect pathway MSNs of the indicated genotypes. (*P < 0.05, Mann-Whitney). Error bars denote s.e.m.

in synapse formation, much of the synaptic development of MSNs occurs postnatally[25], and the maintained expression of *Plxnd1* suggests that the receptor regulates later phases of synapse formation. To demonstrate a postnatal function of Plexin-D1, we postnatally deleted *Plxnd1* using infection with adeno-associated virus (AAV) encoding a Cre-mCherry red fluorescent protein fusion construct (AAV-Cre-mCherry). AAV-Cre-mCherry was stereotactically injected into the striatum of P4–5 *Drd2-GFP;Plxnd1f/f* mice or *Drd2-GFP;Plxnd1f/+* littermate controls (**Fig. 6a**). ISH 4–6 d after unilateral injection revealed substantial downregulation of *Plxnd1* in the infected areas of *Plxnd1f/f* mice (**Supplementary Fig. 7**).

We examined synaptic strength and spine density in direct and indirect pathway MSNs 2 to 3 weeks after AAV-Cre-mCherry injection. Data were collected from spiny GFP-positive and GFP-negative neurons that showed distinct red fluorescence in the nucleus, indicating expression of the Cre-mCherry fusion (**Fig. 6b,c**). Electrophysiological analysis in these mice revealed phenotypes that were essentially identical to those of the *Plxnd1* direct-pathway-specific conditional knockout mice: increased frequency of mEPSCs in *Plxnd1* mutant direct pathway MSNs (control, 1.31 ± 0.18 Hz, n = 12; *Plxnd1* null, 2.16 ± 0.27 Hz, n = 11; P < 0.05, Mann-Whitney) without significant differences in amplitude (control, 13.2 ± 1.1 pA; *Plxnd1* null, 13.2 ± 0.67 pA; P > 0.05, Mann-Whitney) (**Fig. 6d,e**). In contrast, in indirect pathway MSNs we saw no difference in mEPSC frequency (control, 2.57 ± 0.58 Hz, n = 7; *Plxnd1* null, 2.32 ± 0.26 Hz, n = 6; P > 0.05, Mann-Whitney) or amplitude (control, 13.8 ± 2.3 pA, n = 7; *Plxnd1* null, 13.4 ± 1.5 pA, n = 6; P > 0.05, Mann-Whitney; **Fig. 6d,f**) after loss of *Plxnd1*. Similarly to what was found in pathway-specific *Plxnd1* conditional null mice (**Fig. 4**), loss of *Plxnd1* decreased spine density ~15% in direct pathway MSNs (control, 0.94 ± 0.04 spines µm^{-1}, n = 37 dendrites in 10 cells; *Plxnd1* null, 0.80 ± 0.04 spines µm^{-1}, n = 37 dendrites in 9 cells; P < 0.05) but had no effect on indirect pathway MSNs (control, 1.06 ± 0.03 spines µm^{-1}, n = 26 dendrites in 7 cells; *Plxnd1* null, 1.09 ± 0.04 spines µm^{-1}, n = 18 dendrites in 6 cells; P > 0.05, Mann-Whitney) (**Fig. 6g,h**). No significant changes in spine length, width and head area were observed between control and *Plxnd1* null MSNs of either pathway (P > 0.05, Mann-Whitney; **Supplementary Fig. 8**). Thus, postnatal loss of *Plxnd1* produced a similar synaptic phenotype—increased mEPSC rate and slightly decreased spine density—in direct pathway MSNs to that of constitutive loss of *Plxnd1* in the direct pathway conditional null mice, demonstrating that Plexin-D1 regulates postnatal synapse formation in direct pathway MSNs.

Sema3E–Plexin-D1 signaling controls synapse specificity

Because *Sema3e* is expressed highly in the thalamus and sparsely in deep layers of the cortex, we examined whether the synaptic alternations observed in *Sema3e* and *Plxnd1* mutant mice reflect defects in
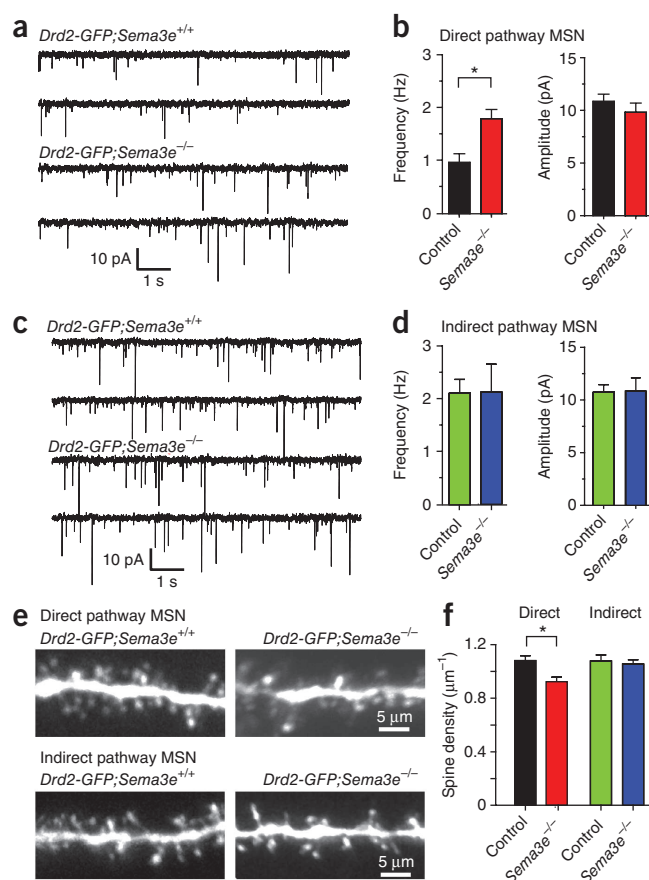
specific subsets of glutamatergic synapses formed onto direct pathway MSNs. Loss of *Plxnd1* in direct pathway MSNs has only little effect on spine number and density while nearly doubling mEPSC frequency, suggesting either that the distribution of synapses onto dendritic spine heads versus those onto aspiny regions of the cell has shifted or that postsynaptic loss of *Plxnd1* increases the probability of release from innervating glutamatergic fibers. Of note, corticostriatal inputs are formed predominantly onto spine heads, whereas only ~50% of thalamostriatal axons form synapses onto spine heads[9,11]. Furthermore, the probability of neurotransmitter release is typically lower at corticostriatal than at thalamostriatal synapses[10]. Therefore, it is possible that postsynaptic loss of *Plxnd1* in direct pathway MSNs selectively triggers an increase in thalamostriatal inputs, which would increase mEPSC rate despite no net changes in total number of spines. To directly test this hypothesis, we separately examined glutamatergic synapses formed onto MSNs by cortical and thalamic axons. Excitatory postsynaptic currents (EPSCs) were recorded in direct and indirect pathway MSNs from direct pathway mutant *Drd2-GFP;Drd1a-cre;Plxnd1f/f* mice and from *Drd2-GFP;Drd1a-cre;Plxnd1f/+* littermate or wild type controls. To achieve specific activation of thalamostriatal axons, AAV encoding fluorophore-tagged Channelrhodopsin-2 (ChR2-mCherry) was injected into the parafasicular nucleus of the thalamus (**Fig. 7a,b**). Three to 4 weeks after virus injection, thalamostriatal axons expressing ChR2-mCherry were prominent in the striatum and could be identified in acute brain slices (**Fig. 7c**).

To detect possible changes in synaptic strength, we recorded EPSCs in neighboring direct and indirect pathway MSNs (<50 µm apart) simultaneously (10 pairs) or sequentially (14 pairs) (**Fig. 7d–i**). In control mice, optogenetic activation of thalamostriatal axons elicited robust EPSCs in direct and indirect pathway MSNs of similar
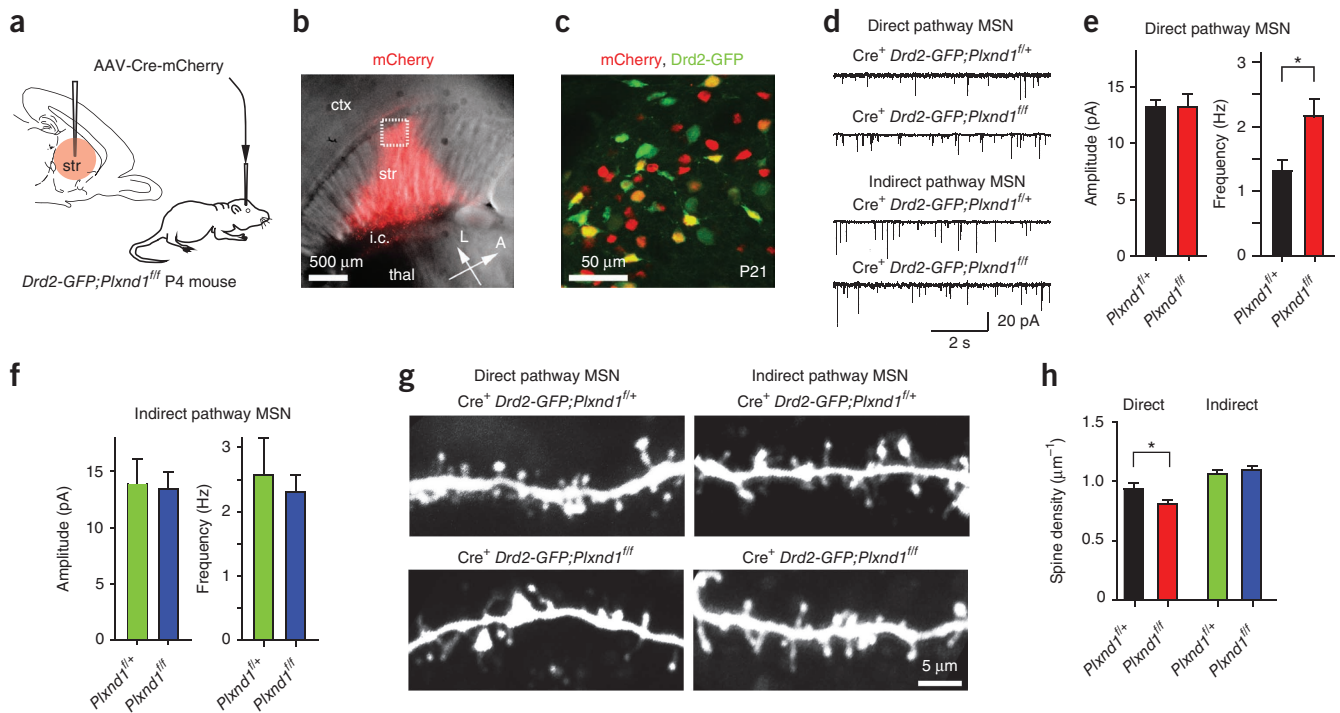
Figure 6 Postnatal deletion of *Plxnd1* perturbs spine density and mEPSC frequency in direct but not indirect pathway MSNs. (**a**) Injection of AAV encoding Cre-mCherry into the striatum (str) of P4–5 *Drd2-GFP;Plxnd1f/f* mice or their littermate controls (*Drd2-GFP;Plxnd1f/+*). (**b**) Brain slices cut 2–3 weeks after virus injection and mCherry fluorescence to confirm Cre expression (right). Ctx, cortex; thal, thalamus; str, striatum; i.c., internal capsule; L, lateral; A, anterior. (**c**) Image of a brain slice from a *Drd2-GFP;Plxnd1f/f* mouse 2 weeks after AAV virus injection showing sparse Cre expression (red) in both GFP-positive (green) and GFP-negative neurons. (**d**) mEPSCs recorded from Cre+ direct and indirect pathway MSNs from *Plxnd1f/f* mice and *Plxnd1f/+* control mice. (**e**,**f**) Summary of changes in mEPSC amplitude (left) and frequency (right) in direct (**e**) and indirect (**f**) pathway MSNs. *$P < 0.05$, Mann-Whitney. (**g**) Images of dendritic segments of Cre-expressing direct and indirect pathway MSNs in mice with one (top) or two (bottom) copies of the conditional *Plxnd1* allele. The Cre+ direct pathway MSNs (red in **c**) in *Plxnd1f/f* mice show lower spine density than those in virus-injected littermate controls (Cre+ *Plxnd1f/+*). In contrast, there is no detectable difference in spine density between Cre+ indirect pathway MSNs (yellow in **c**) in *Plxnd1f/f* and *Plxnd1f/+* littermate control mice. (**h**) Summary of changes in direct and indirect pathway MSNs showing a significant difference in spine density between Cre+ *Plxnd1f/f* direct pathway MSNs and Cre+ *Plxnd1f/+* heterozygous controls (*$P < 0.05$, Mann-Whitney). Error bars denote s.e.m.

amplitudes (EPSC ratio direct/indirect, 0.99 ± 0.11; $n = 6$ pairs; **Fig. 7d,e**), suggesting that thalamic neurons similarly innervate both MSN classes. In contrast, in direct pathway mutant mice, we observed larger evoked thalamostriatal EPSCs in direct pathway MSNs than in neighboring indirect pathway MSNs (EPSC ratio direct/indirect, 1.83 ± 0.26, $n = 6$ pairs; $P < 0.05$ compared to control; **Fig. 7d,e**). Paired-pulse stimulation at a 50-ms inter-stimulus interval with blue light yielded no change in paired-pulse ratios (direct pathway control, 0.61 ± 0.10, $n = 6$; direct pathway mutant, 0.44 ± 0.16, $n = 6$; $P > 0.05$, Mann-Whitney; indirect pathway control, 0.27 ± 0.10; direct pathway mutant, 0.39 ± 0.07, $n = 6$; $P > 0.05$, Mann-Whitney). Therefore, loss of *Plxnd1* in direct pathway MSNs enhanced thalamostriatal synaptic strength in direct pathway MSNs relative to that in indirect pathway MSNs.

Similar analysis using electrical stimulation of corticostriatal inputs revealed that cortically evoked EPSCs had similar amplitudes in neighboring direct and indirect pathway MSNs of control mice (EPSC ratio direct/indirect, 1.05 ± 0.17; $P > 0.05$, $n = 6$ pairs, Wilcoxon) (**Fig. 7f,g**). However, in contrast to the above findings, we did not observe significant differences in evoked corticostriatal EPSCs between direct and indirect pathway MSNs from direct pathway mutant mice (EPSC ratio direct/indirect, 1.05 ± 0.08; $P > 0.05$, $n = 6$ pairs, Wilcoxon). In addition, paired-pulse stimuli revealed no changes in paired-pulse ratios between control and mutant MSNs (direct pathway control, 1.44 ± 0.36, $n = 6$; direct pathway mutant, 1.08 ± 0.11, $n = 6$; $P > 0.05$,

Mann-Whitney; indirect pathway control, 1.13 ± 0.11, $n = 6$; direct pathway mutant, 1.05 ± 0.09, $n = 6$; $P > 0.05$, Mann-Whitney).

To exclude the possibility that electrical stimulation could not reveal subtle changes in corticostriatal transmission, we stimulated corticostriatal inputs using ChR2. We injected AAV encoding ChR2-mCherry into motor cortex and recorded pairs of direct and indirect pathway MSNs 4 weeks after virus injection. Optogenetic activation of corticostriatal axons evoked similar-size EPSCs in direct and indirect pathway MSNs from control and direct pathway mutant mice (control EPSC ratio direct/indirect. 1.05 ± 0.03, $n = 7$ pairs; $P > 0.05$, Wilcoxon; direct pathway mutant EPSC ratio direct/indirect, 0.94 ± 0.06, $n = 5$ pairs; $P > 0.05$, Wilcoxon) (**Fig. 7h,i**). Thus, postsynaptic expression of *Plxnd1* in direct pathway MSNs selectively controls synaptic strength of thalamostriatal but not corticostriatal inputs. Specifically, Sema3E–Plexin-D1 signaling negatively regulates synaptic strength of thalamostriatal synapses onto direct pathway MSNs. Such changes in direct pathway *Plxnd1* mutant mice enhance the excitatory drive from thalamus to the direct pathway[26], possibly contributing to reduced basal locomotion and exploration of the central open area of an arena seen in direct pathway *Plxnd1* mutant mice (**Supplementary Fig. 9**).

Loss of *Plxnd1* increases thalamostriatal synapse number

To directly test whether the number of thalamostriatal synapses onto direct pathway MSNs increased in the absence of Plexin-D1,
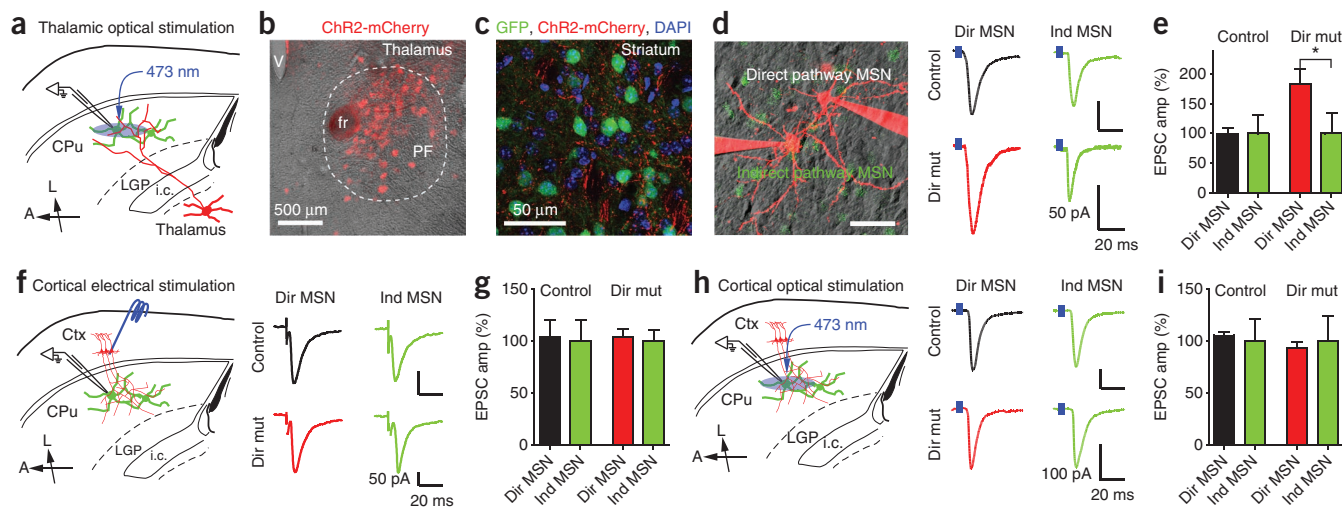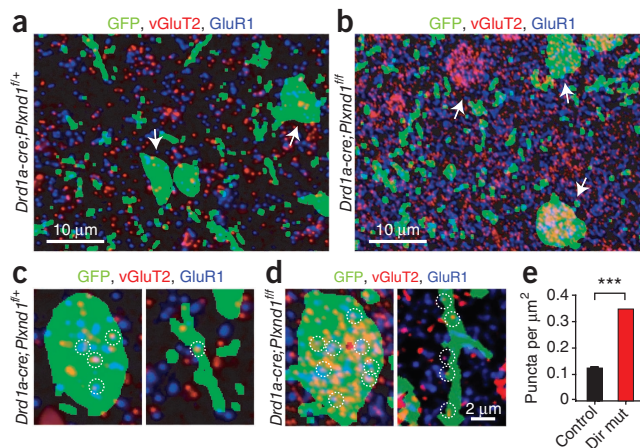
Figure 7 Loss of *Plxnd1* in direct pathway MSNs selectively increases the strength of thalamostriatal glutamatergic inputs. (**a**) Schematic of the recording configuration. Blue, 473-nm blue light; i.c., internal capsule; CPu, caudate putamen, LGP, lateral globus pallidus. (**b**) Image of a 50-μm-thick coronal slice showing ChR2-mCherry expression in the parafascicular (PF) nucleus of the thalamus. Fasciculus retroflexus, fr. (**c**) Confocal image of thalamostriatal axons expressing ChR2-mCherry (red) and GFP (green) in the striatum of a *Drd2-GFP;Drd1a-cre;Plxnd1^{f/+}* mouse. (**d**) Left, 2PLSM image of direct and indirect pathway MSNs under simultaneous whole-cell voltage-clamp. Right, examples of blue light–evoked thalamostriatal EPSCs recorded from neighboring direct (dir) and indirect (ind) pathway MSNs in *Drd2-GFP;Drd1a-cre;Plxnd1^{f/f}* conditional knockout mice (mut) and their littermate control mice. (**e**) Summary of normalized thalamostriatal EPSCs amplitudes (amp). (**f**) Left, recording configuration (ctx, cortex). Right, examples of evoked corticostriatal EPSCs recorded simultaneously in neighboring direct and indirect pathway MSNs from a *Drd2-GFP;Drd1a-cre;Plxnd1^{f/f}* mouse and a littermate control. (**g**) Summary of normalized corticostriatal EPSC amplitudes in direct and indirect pathway MSNs. (**h**) Left, recording configuration. Right, examples of evoked corticostriatal EPSCs recorded simultaneously in neighboring direct and indirect pathway MSNs from a *Drd2-GFP;Drd1a-cre;Plxnd1^{f/f}* mouse and a littermate control. (**i**) Summary of normalized corticostriatal EPSC amplitudes in direct and indirect pathway MSNs. L, lateral; A, anterior. *$P < 0.05$; Wilcoxon. Error bars denote s.e.m.

we performed immunohistochemical analysis of vGluT2, a presynaptic marker found in thalamic but not cortical axons, and GluR1, a component of postsynaptic AMPA-type glutamate receptors. Quantitation of the number of thalamostriatal synapses was performed in ultrathin (100 nm) slices, which substantially improves the resolution and reduces superimposition of fluorescent puncta in different focal planes[27]. To mark a sparse subset of direct pathway MSNs with a space-filling fluorophore, we injected AAV carrying double-floxed inverted GFP into the striatum of het ctrl (*Drd1a-cre;Plxnd1^{f/+}*) and direct pathway mutant (*Drd1a-cre;Plxnd1^{f/f}*) mice. It is necessary to use sparse labeling, as marking all direct pathway MSNs results in a dense background of green fluorescence. However, this approach constrains the analysis to GFP-expressing neurons because unlabeled MSNs cannot be unambiguously assigned to the direct or indirect pathway.

Putative thalamostriatal synapses were identified as closely apposed presynaptic (vGluT2-positive) and postsynaptic (GluR1-positive) puncta (**Fig. 8**). We observed an increase in such puncta (**Fig. 8a,b**) in direct pathway mutant mice compared to controls. Furthermore, only a small number of vGluT2-positive puncta were found on the somata of control direct pathway MSNs, whereas vGluT2-postive puncta densely covered the somata of mutant direct pathway MSNs (**Fig. 8c,d**). Automated image analysis indicated that the density of colocalized GluR1-vGluT2 puncta that overlapped with GFP-positive regions was significantly greater ($P < 0.0001$, Mann-Whitney) in direct pathway mutant mice (0.347 ± 0.007 μm^{-2}, $n = 236$ sections in 8 slices) compared to control (0.125 ± 0.004 μm^{-2}, $n = 320$ sections in 9 slices) (**Fig. 8e**). Thus, the number of immunohistochemically identified putative thalamostriatal synapses was increased in *Plxnd1* null direct pathway MSNs, further

Figure 8 Loss of *Plxnd1* in direct pathway MSNs increases the number of vGluT2 and GluR1 positive puncta on direct pathway MSNs. (**a,b**) Single-plane array tomography images of a 100-nm striatal section showing GFP (green) expressed in a sparse subset of direct pathway MSNs, vGluT2 (red) and GluR1 (blue) in the striatum from control (**a**) and direct pathway *Plxnd1* mutant mice (**b**). Arrows highlight formation of thalamostriatal synapses around somatic regions of MSNs. (**c,d**) High-magnification images from control (**c**) and direct pathway *Plxnd1* mutant mice (**d**) showing the puncta distribution on soma (left) and dendrite (right) of direct pathway MSNs (green). Thalamostriatal synapses are defined by the close apposition of presynaptic (vGluT2) and postsynaptic (GluR1) markers (examples highlighted in white circles). In **a–c**, green indicates the segmented areas of GFP fluorescence that were used to identify sections of direct pathway MSNs. (**e**) Quantification of the density of putative thalamic synapses formed on direct pathway MSNs in control and direct pathway *Plxnd1* mutant mice. ***$P < 0.0001$, Mann-Whitney. Error bars denote s.e.m.

supporting the conclusion that Sema3E–Plexin-D1 signaling normally inhibits thalamostriatal synapse formation. Furthermore, the dense perisomatic innervation in the direct pathway mutant mice likely contributes to the markedly increased mEPSC rate in the mutant mice, as somatic synapses are electronically close to the recording electrode and are therefore detected at a higher rate than synapses formed onto thin dendrites.

DISCUSSION

Our results demonstrate that the specificity of glutamatergic synaptic connectivity in the striatum is controlled by target- and source-specific expression of a ligand-receptor pair, Sema3E and Plexin-D1. Plexin-D1 is selectively expressed in direct but not in indirect pathway MSNs and thereby provides a mechanism to control synapse formation in a subset of functionally distinct but anatomically intermixed postsynaptic neurons. The ligand, secreted Sema3E, is highly expressed in the thalamus but only sparsely expressed in deep layers of cortex[28], which allows selective action on synapses between a particular pair of neuronal classes. Disruption of Sema3E–Plexin-D1 signaling *in vivo* results in functional and anatomical rearrangement of thalamostriatal synapses specifically in direct pathway MSNs without affecting the strength of corticostriatal innervation. Together the thalamic expression of *Sema3e* and direct pathway–specific expression of *Plxnd1* underlie a molecular recognition mechanism that selectively restricts thalamostriatal synapse formation.

Our understanding of the molecular mechanisms of synapse specificity has mainly come from studies of brain areas in which neurons of a specific class are organized into well defined subdivisions[14,16–18]. For example, in the inner plexiform layer of the mouse retina, transmembrane semaphorin 6A is expressed in ON sublamina and its receptor Plexin-A4 is expressed in adjacent OFF sublamina. The repulsive nature of the interaction between these transmembrane proteins ensures that Plexin-A4 -positive axons do not innervate the ON sublamina and results in lamina-specific neurite stratification[17]. Similarly, in the mouse spinal cord, Sema3E secreted by neurons of the cutaneous maximus motor pool signals through Plexin-D1 expressed by a subset of proprioceptive afferents to repel these axons[18]. In both examples, anatomically clustered postsynaptic neurons express repulsive ligands that prevent innervation by inappropriate axons. However, in the striatum, cortical and thalamic axons as well as direct and indirect pathway MSNs are intermixed, rendering establishment of a uniform repellent signal by target neurons insufficient to direct synapse selection. Notably, in thalamostriatal projections the orientation of receptor and ligand expression is reversed, such that Sema3E is secreted by axons and Plexin-D1 is expressed by one subtype of postsynaptic neuron. Therefore, although the protein families of the receptor-ligand pair are conserved, the logic of establishing synapse specificity in the striatum is different from that previously described in the retina and spinal cord.

The electrophysiological and anatomical data presented here indicate that Sema3E–Plexin-D1 signaling negatively regulates thalamostriatal synapse formation. Of note, this regulation is graded in the sense that *Plxnd1* expression modulates the strength of thalamic inputs, rather than rejecting all inputs from the thalamus. Furthermore, the increase in mEPSC rate without large changes in spine density, dendritic arborization or corticostriatal synaptic strength suggest that loss of Sema3E–Plexin-D1 signaling increases the number of thalamostriatal glutamatergic synapses formed onto the somata and the dendritic shafts of direct pathway MSNs. This possibility is supported by estimates of thalamostriatal synapse density in direct pathway MSNs using array tomography–based immunohistochemical analysis (**Fig. 8**). This specificity may arise by selective localization of Plexin-D1 protein to a subcellular compartment of the direct pathway MSNs. Indeed, previous studies have shown that both neuropilins and Plexin-A2 are expressed with inhomogeneous subcellular distributions[29,30].

Despite the consistent small decrease in dendritic spine density of direct pathway MSNs seen upon the loss of *Plxnd1* or *Sema3e*, we were unable to detect a significant change in corticostriatal innervation of these cells. This may be because spine density is a measure of synapse density on the dendrite, whereas the amplitudes of evoked synaptic currents are proportional to the total number of synapses formed onto the cell. Therefore, the changes to the dendrites of *Plxnd1*-lacking neurons might leave total synapse number relatively unaffected despite a decrease in synapse density. Furthermore, a difficult-to-detect small reduction of corticostriatal transmission would be in contrast to the strengthening of thalamostriatal synapses, indicating input-specific regulation of synapse formation in the striatum.

Because secreted Sema3E is expressed by thalamostriatal axons, it is unlikely that Sema3E–Plexin-D1 signaling directly affects the targeting of the axon. Instead, Sema3E–Plexin-D1 signaling may control thalamostriatal synaptic strength by regulating the receptivity of direct pathway MSNs to thalamic inputs, such as by triggering postsynaptic signaling cascades that alter the cytoskeleton or regulate glutamate receptor trafficking and stabilization. For example, the small GTPases Rac and Rho are involved in Plexin-B1 function[31] and regulate synapse and spine formation in many neuron classes[31,32]. An alternative model is that Sema3E-dependent activation of postsynaptic Plexin-D1 may induce production of a retrograde signal that repels thalamostriatal axons[33–35].

The proper balance of excitatory synapses formed by cortical and thalamic neurons onto direct and indirect pathway MSNs is crucial for a variety of behaviors, such as locomotion, anxiety, attention orientation, motor learning and reward[36–38]. The thalamostriatal pathway has been suggested to mediate salient environmental information and regulate motor behavior[39,40]. Consistent with our results showing an increased number of thalamostriatal synapses, we observed changes in basal locomotor behavior in *Plxnd1* direct pathway mutant mice (**Supplementary Fig. 9**). Direct pathway mutant mice traveled less distance than controls, showed longer delays to enter the central open quadrant of an area and spent less time in that quadrant, suggesting that changes in thalamostriatal synapses can lead to increased anxiety and decreased basal locomotion.

METHODS

Methods and any associated references are available in the online version of the paper at http://www.nature.com/natureneuroscience/.

Note: Supplementary information is available on the Nature Neuroscience website.

1. Sanes, J.R. & Yamagata, M. Many paths to synaptic specificity. *Annu. Rev. Cell Dev. Biol.* **25**, 161–195 (2009).
2. Williams, M.E., de Wit, J. & Ghosh, A. Molecular mechanisms of synaptic specificity in developing neural circuits. *Neuron* **68**, 9–18 (2010).
3. Surmeier, D.J., Ding, J., Day, M., Wang, Z. & Shen, W. D1 and D2 dopamine-receptor modulation of striatal glutamatergic signaling in striatal medium spiny neurons. *Trends Neurosci.* **30**, 228–235 (2007).
4. Albin, R.L., Young, A.B. & Penney, J.B. The functional anatomy of basal ganglia disorders. *Trends Neurosci.* **12**, 366–375 (1989).
5. Wichmann, T. & DeLong, M.R. Functional and pathophysiological models of the basal ganglia. *Curr. Opin. Neurobiol.* **6**, 751–758 (1996).
6. Wilson, C.J. Basal ganglia. in *The Synaptic Organization of the Brain* (ed. Shepherd, G.M.) 361–414 (Oxford Univ. Press, 2004).
7. Surmeier, D.J., Song, W.J. & Yan, Z. Coordinated expression of dopamine receptors in neostriatal medium spiny neurons. *J. Neurosci.* **16**, 6579–6591 (1996).
8. Kawaguchi, Y., Wilson, C.J. & Emson, P.C. Intracellular recording of identified neostriatal patch and matrix spiny cells in a slice preparation preserving cortical inputs. *J. Neurophysiol.* **62**, 1052–1068 (1989).
9. Smith, Y., Raju, D.V., Pare, J.F. & Sidibe, M. The thalamostriatal system: a highly specific network of the basal ganglia circuitry. *Trends Neurosci.* **27**, 520–527 (2004).
10. Ding, J., Peterson, J.D. & Surmeier, D.J. Corticostriatal and thalamostriatal synapses have distinctive properties. *J. Neurosci.* **28**, 6483–6492 (2008).
11. Doig, N.M., Moss, J. & Bolam, J.P. Cortical and thalamic innervation of direct and indirect pathway medium-sized spiny neurons in mouse striatum. *J. Neurosci.* **30**, 14610–14618 (2010).
12. Raju, D.V., Shah, D.J., Wright, T.M., Hall, R.A. & Smith, Y. Differential synaptology of vGluT2-containing thalamostriatal afferents between the patch and matrix compartments in rats. *J. Comp. Neurol.* **499**, 231–243 (2006).
13. Yamagata, M. & Sanes, J.R. Synaptic localization and function of Sidekick recognition molecules require MAGI scaffolding proteins. *J. Neurosci.* **30**, 3579–3588 (2010).
14. Yamagata, M., Weiner, J.A. & Sanes, J.R. Sidekicks: synaptic adhesion molecules that promote lamina-specific connectivity in the retina. *Cell* **110**, 649–660 (2002).
15. Shen, K., Fetter, R.D. & Bargmann, C.I. Synaptic specificity is generated by the synaptic guidepost protein SYG-2 and its receptor, SYG-1. *Cell* **116**, 869–881 (2004).
16. Yamagata, M. & Sanes, J.R. Dscam and Sidekick proteins direct lamina-specific synaptic connections in vertebrate retina. *Nature* **451**, 465–469 (2008).
17. Matsuoka, R.L. *et al.* Transmembrane semaphorin signalling controls laminar stratification in the mammalian retina. *Nature* **470**, 259–263 (2011).
18. Pecho-Vrieseling, E., Sigrist, M., Yoshida, Y., Jessell, T.M. & Arber, S. Specificity of sensory-motor connections encoded by Sema3e-Plxnd1 recognition. *Nature* **459**, 842–846 (2009).
19. Chauvet, S. *et al.* Gating of Sema3E/PlexinD1 signaling by neuropilin-1 switches axonal repulsion to attraction during brain development. *Neuron* **56**, 807–822 (2007).
20. Fiala, J.C., Feinberg, M., Popov, V. & Harris, K.M. Synaptogenesis via dendritic filopodia in developing hippocampal area CA1. *J. Neurosci.* **18**, 8900–8911 (1998).
21. Rakic, P., Bourgeois, J.P., Eckenhoff, M.F., Zecevic, N. & Goldman-Rakic, P.S. Concurrent overproduction of synapses in diverse regions of the primate cerebral cortex. *Science* **232**, 232–235 (1986).
22. Alvarez, V.A. & Sabatini, B.L. Anatomical and physiological plasticity of dendritic spines. *Annu. Rev. Neurosci.* **30**, 79–97 (2007).
23. Heintz, N. BAC to the future: the use of bac transgenic mice for neuroscience research. *Nat. Rev. Neurosci.* **2**, 861–870 (2001).
24. Gu, C. *et al.* Semaphorin 3E and plexin-D1 control vascular pattern independently of neuropilins. *Science* **307**, 265–268 (2005).
25. Jacobs, E.C. *et al.* Visualization of corticofugal projections during early cortical development in a tau-GFP-transgenic mouse. *Eur. J. Neurosci.* **25**, 17–30 (2007).
26. Ding, J.B., Guzman, J.N., Peterson, J.D., Goldberg, J.A. & Surmeier, D.J. Thalamic gating of corticostriatal signaling by cholinergic interneurons. *Neuron* **67**, 294–307 (2010).
27. Micheva, K.D. & Smith, S.J. Array tomography: a new tool for imaging the molecular architecture and ultrastructure of neural circuits. *Neuron* **55**, 25–36 (2007).
28. Watakabe, A., Ohsawa, S., Hashikawa, T. & Yamamori, T. Binding and complementary expression patterns of semaphorin 3E and plexin D1 in the mature neocortices of mice and monkeys. *J. Comp. Neurol.* **499**, 258–273 (2006).
29. Suto, F. *et al.* Interactions between plexin-A2, plexin-A4, and semaphorin 6A control lamina-restricted projection of hippocampal mossy fibers. *Neuron* **53**, 535–547 (2007).
30. Tran, T.S. *et al.* Secreted semaphorins control spine distribution and morphogenesis in the postnatal CNS. *Nature* **462**, 1065–1069 (2009).
31. Vikis, H.G., Li, W. & Guan, K.L. The plexin-B1/Rac interaction inhibits PAK activation and enhances Sema4D ligand binding. *Genes Dev.* **16**, 836–845 (2002).
32. Luo, L. Rho GTPases in neuronal morphogenesis. *Nat. Rev. Neurosci.* **1**, 173–180 (2000).
33. Fox, M.A. *et al.* Distinct target-derived signals organize formation, maturation, and maintenance of motor nerve terminals. *Cell* **129**, 179–193 (2007).
34. Terauchi, A. *et al.* Distinct FGFs promote differentiation of excitatory and inhibitory synapses. *Nature* **465**, 783–787 (2010).
35. Johnson-Venkatesh, E.M. & Umemori, H. Secreted factors as synaptic organizers. *Eur. J. Neurosci.* **32**, 181–190 (2010).
36. Graybiel, A.M., Aosaki, T., Flaherty, A.W. & Kimura, M. The basal ganglia and adaptive motor control. *Science* **265**, 1826–1831 (1994).
37. Wickens, J.R., Reynolds, J.N. & Hyland, B.I. Neural mechanisms of reward-related motor learning. *Curr. Opin. Neurobiol.* **13**, 685–690 (2003).
38. Schultz, W. Behavioral theories and the neurophysiology of reward. *Annu. Rev. Psychol.* **57**, 87–115 (2006).
39. Matsumoto, N., Minamimoto, T., Graybiel, A.M. & Kimura, M. Neurons in the thalamic CM-Pf complex supply striatal neurons with information about behaviorally significant sensory events. *J. Neurophysiol.* **85**, 960–976 (2001).
40. Minamimoto, T. & Kimura, M. Participation of the thalamic CM-Pf complex in attentional orienting. *J. Neurophysiol.* **87**, 3090–3101 (2002).

ONLINE METHODS

Mice. *Plxnd1^{flox/flox}* (*Plxnd1^{f/f}*) mice[41] and *Sema3e* knock out (*Sema3e^{−/−}*) mice[24] were maintained on a C57BL/6 background. *Plxnd1^{+/−}* mice[24] were maintained on Swiss Webster background. *Drd1a-GFP*, *Drd2-GFP*, *Drd1a-cre* and *Drd2-GFP* mice, which express enhanced green fluorescent protein (EGFP) or Cre recombinase under the control of the type 1a (D1R) and type 2 (D2R) dopamine receptor promoter using a bacterial artificial chromosome (BAC) containing *Drd1a* and *Drd2* loci (GENSAT), were maintained on a mixed background of C57BL/6 and FVB (GENSAT). Swiss Webster and C57BL/6 wild-type mice were obtained from Taconic Farms. Conditional deletion of *Plxnd1* was achieved by breeding *Plxnd1^{f/f}* mice to *Drd1a-cre* or *Drd2-cre* transgenic mice. To visualize direct and indirect pathway MSNs, *Drd2-GFP;Drd1a* (or *Drd2)-cre;Plxnd1^{f/+}* mice and their littermates were generated by breeding *Drd2-GFP;Plxnd1^{f/+}* mice with *Drd1a* (or *Drd2)-cre;Plxnd1^{f/+}* mice. All animals were treated according to institutional and US National Institutes of Health guidelines approved by the Institutional Animal Care and Use Committee at Harvard Medical School. Approximately 400 mice, with equal numbers of males and females, were used in this study.

Stereotaxic virus injection and retrograde dye labeling. To knock out *Plxnd1* expression postnatally, an adeno-associated virus (AAV, serotype 1) encoding Cre was injected into *Plxnd1^{f/f}* mice[42]. P4–5 *Plxnd1^{f/f}* mice were anesthetized with isoflurane and mounted on a stereotaxic frame (Stoelting) equipped with ear cups (Kopf). An AAV-Cre-mCherry virus (1.0 μl of 1.2×10^{13} genome copy ml^{−1} diluted 1:2 in PBS) was injected at a rate of 100 nl min^{−1} unilaterally into the striatum region. The viral backbone construct was kindly provided by M. During (Ohio State University)[42]. Mice were used for experiments 14–21 d after virus injection.

The AAV construct carrying a double-floxed inverted ChR2-mCherry cassette was kindly provided by K. Deisseroth (Stanford University)[43]. To construct an AAV vector that expressed ChR2-mCherry in the absence of Cre, the DNA cassette carrying two pairs of incompatible lox sites (*loxP* and *lox2722*) was synthesized and the ChR2-mCherry transgene was inserted in the forward, coding orientation between the *loxP* and *lox2722* sites. AAV-ChR2-mCherry (1.0 μl) was injected into the parafascicular region in the thalamus of *Drd2-GFP;Plxnd1^{f/f}; Drd1a-Cre* mice and their littermates to express ChR2 in thalamic neurons. Mice were used for experiments 14–21 d after virus injection. Viruses were prepared by the Harvard Gene Therapy Initiative or the Gene Therapy Center at University of North Carolina at Chapel Hill. To retrogradely label neurons sending axons into the striatum, 50 nl of 20% (wt/vol) 4′,6-diamidino-2-phenylindole dihydrochloride (DiI, Sigma) dissolved in dimethylsulfoxide was injected stereotaxically into dorsal striatum of P3 wild-type pups as described above. After 48 h, brains were cryosectioned and imaged to visualize labeled cells. ISH was subsequently performed in adjacent sections from the same brain and images were overlaid with DiI-traced images using DAPI staining.

Histology. Nonradioactive ISH was performed according to standard methods[24]. Briefly, brains from neonatal pups were dissected in PBS and immediately frozen by dipping in liquid nitrogen several times. In some cases, brains were fixed by transcardial perfusion with PBS, pH 7.4, followed by 4% (wt/vol) paraformaldehyde (PFA) and postfixed overnight at 4 °C in 4% PFA. The fixed brains were cryoprotected in 30% (wt/vol) sucrose in PBS and frozen on dry ice. Brains were cut in 16-μm-thick sections with a cryostat (Leica), postfixed in 4% PFA, acetylated in 1% (vol/vol) triethanolamine and 0.25% (vol/vol) acetic anhydride, prehybridized, and hybridized at 65 °C using the following anti-sense probes: *Plxnd1* (NM_026376.3, nt381-1334), *EGFP* (U55761, nt159-754), *Sema3e*[24]. After hybridization, sections were washed and incubated with alkaline phosphatase–conjugated sheep antibody to digoxigenin for 90 min at room temperature (22–23 °C). After several washes, sections were incubated in BM Purple (Roche) until positive staining was detected. Double fluorescence *in situ* hybridization was performed using tyramide signal amplification method according to the manufacturer's instructions (PerkinElmer). Two fluorescein- or digoxigenin-labeled antisense probes were hybridized simultaneously and stained by fluorescein or Cy3 chromogens, respectively.

Electrophysiology and two-photon laser scanning microscopy. Parasagittal or oblique horizontal acute brain slices (275–300 μm) were obtained from mice 18–28 d old using standard techniques[10]. Individual slices were transferred to a submersion-style recording chamber and continuously superfused with artificial cerebrospinal fluid at a rate of 2–3 ml min^{−1} at room temperature (22–23 °C). The artificial cerebrospinal fluid contained the following (in mM): 125 NaCl, 2.5 KCl, 2 CaCl_2, 1 MgCl_2, 25 NaHCO_3, 1.25 NaH_2PO_4 and 12.5 glucose. Whole-cell voltage-clamp recordings were performed using standard techniques. Pipettes (3–5 MΩ) were filled with either a Cs^+-based solution containing (in mM) 120 cesium methanesulfonate, 15 CsCl, 8 NaCl, 10 tetraethyl-ammonium chloride, 10 HEPES, 2–5 QX-314, 0.2 EGTA, 2 Mg-ATP, 0.3 Na-GTP, pH 7.3 adjusted with CsOH. For all experiments, 10 μM (−)SR95531 (gabazine) or 50 μM picrotoxin was added to the superfusion medium to block GABA_A receptor–mediated synaptic responses. For recording miniature EPSCs (mEPSCs), D-2-amino-5-phosphonovaleric acid (D-AP5, 10 μM) was added to block NMDA receptor–mediated currents and TTX was included to prevent action potential firing. Recordings were obtained with a Multiclamp 700B (filter set at 2–5 kHz); signals were digitized at 10 kHz. For evoked EPSCs, TTX was omitted and stimulation (50–200 μs) was performed using steel concentric electrodes (Frederick Haer & Co.). The cortical afferents were stimulated by placing the stimulation electrode between layers V and VI in the cortex. To stimulate ChR2-expressing axons, 473 nm blue laser light (5 ms pulses, 2–10 mW entering the objective) was focused on the back focal plane of the objective, creating a near-collimated beam through the sample. 2PLSM was accomplished using a custom-made microscope described previously[44,45].

Array tomography. Four mice (two mutant *Drd1a-cre;Plxnd1^{f/f}* and two het ctrl *Drd1a-cre;Plxnd1^{f/+}* littermates), P30, were used for array tomography. Brain slices were cut and fixed with 4% PFA in PBS. The tissue was then processed for array tomography as described previously[27]. In brief, the dorsal striatum tissue was dissected, then dehydrated in ethanol and embedded in LRWhite resin (Electron Microscopy Sciences). Serial ultrathin sections (100 nm) were cut on an ultramicrotome (Leica), mounted on cover glasses (24 × 60 mm) and immunostained using vGluT2 (Millipore AB2251) and GluR1 (Millipore AB1504) antibodies. For secondary antibodies, Alexa Fluor-594 and Alexa Fluor-633 conjugates from appropriate species were used. To minimize variability and ensure identical conditions for immunostaining, ribbons of control and mutant tissues were mounted on the same glass slide and processed together. Sections were mounted using antifade reagent with DAPI (Invitrogen). Imaging was done on a Zeiss Apotome fluorescence microscope using a Zeiss ×63, 1.4 numerical aperture objective.

Open field testing of basal locomotor activity. Mice were placed in a 44 cm long × 44 cm wide × 50 cm high open-field chamber. Locomotor activity was recorded for 60 min using an overhead digital camera. The mouse position in the open field was tracked using EthoVision (Noldus).

Data analysis and statistics methods. Imaging and physiology data were acquired using National Instruments boards and custom software written in Matlab (MathWorks)[44]. Offline analysis was performed in Matlab, Igor Pro 6.0 (WaveMetrics) and ImageJ (NIH). Spine morphology was analyzed using custom software written in Matlab[45,46]. Statistical analyses were performed using Prism4 (GraphPad Software). Scholl's concentric analysis was used to quantitatively evaluate the dendritic branching pattern: the number of dendritic intersections in somatically centered circles of increasing radius was counted. Scholl analysis was performed using SynD[47]. Summary data are reported as mean ± s.e.m. Nonmatched samples were analyzed with the nonparametric Mann-Whitney rank sum test. Matched samples were analyzed with Wilcoxon signed ranks test. $P < 0.05$ was considered statistically significant.

Reagents and chemicals. All reagents were obtained from Sigma except Na_2-GTP (Roche) and SR95531 and D-AP5 (Tocris).

41. Zhang, Y. *et al.* Tie2Cre-mediated inactivation of plexinD1 results in congenital heart, vascular and skeletal defects. *Dev. Biol.* **325**, 82–93 (2009).
42. Lu, W. *et al.* Subunit composition of synaptic AMPA receptors revealed by a single-cell genetic approach. *Neuron* **62**, 254–268 (2009).
43. Tsai, H.C. *et al.* Phasic firing in dopaminergic neurons is sufficient for behavioral conditioning. *Science* **324**, 1080–1084 (2009).

44. Pologruto, T.A., Sabatini, B.L. & Svoboda, K. ScanImage: flexible software for operating laser scanning microscopes. *Biomed. Eng. Online* **2**, 13 (2003).

45. Steiner, P. *et al.* Destabilization of the postsynaptic density by PSD-95 serine 73 phosphorylation inhibits spine growth and synaptic plasticity. *Neuron* **60**, 788–802 (2008).

46. Ding, J.B., Takasaki, K.T. & Sabatini, B.L. Supraresolution imaging in brain slices using stimulated-emission depletion two-photon laser scanning microscopy. *Neuron* **63**, 429–437 (2009).

47. Schmitz, S.K. *et al.* Automated analysis of neuronal morphology, synapse number and synaptic recruitment. *J. Neurosci. Methods* **195**, 185–193 (2011).